# Characterization of Plaques Using $^{18}$F-FDG PET/CT in Patients with Carotid Atherosclerosis and Correlation with Matrix Metalloproteinase-1

Yen-Wen Wu[1–3], Hsian-Li Kao[1], Ming-Fong Chen[1], Bai-Chin Lee[1], Wen-Yih I. Tseng[4,5], Jiann-Shing Jeng[6], Kai-Yuan Tzen[2], Ruoh-Fang Yen[2], Por-Jau Huang[1], and Wei-Shiung Yang[1,3,7]

*[1]Department of Internal Medicine, National Taiwan University Hospital, Taipei, Taiwan; [2]Department of Nuclear Medicine, National Taiwan University Hospital, Taipei, Taiwan; [3]Graduate Institute of Clinical Medicine, College of Medicine, National Taiwan University, Taipei, Taiwan; [4]Department of Medical Imaging, National Taiwan University Hospital, Taipei, Taiwan; [5]Center for Optoelectronic Biomedicine, College of Medicine, National Taiwan University, Taipei, Taiwan; [6]Department of Neurology, National Taiwan University Hospital, Taipei, Taiwan; and [7]Institute of Biomedical Sciences, Academia Sinica, Taipei, Taiwan*

High tissue matrix metalloproteinase (MMP) activity has been associated with advanced atherosclerosis and plaque rupture. $^{18}$F-FDG uptake has been reported to detect inflammation. This investigation examined the vascular $^{18}$F-FDG uptake by PET/CT and its correlation with circulating MMP-1 levels. **Methods:** We examined 25 consecutive patients with significant carotid stenosis and 22 healthy control subjects using $^{18}$F-FDG PET/CT. The leukocyte counts, C-reactive protein (CRP), and MMP-1 were measured. **Results:** $^{18}$F-FDG arterial uptake, as well as calcifications, was significantly higher in extensive distributions in patients with established carotid stenosis. However, their distribution was not consistently overlapping. The values of circulating MMP-1 and leukocyte counts were significantly higher in patients with carotid stenosis (all $P < 0.05$). In addition, subjects with higher $^{18}$F-FDG uptake (maximum SUV $> 2.0$) in target lesions had higher baseline and poststenting MMP-1 levels (all $P < 0.05$). **Conclusion:** We provide a link between $^{18}$F-FDG uptake and circulating MMP-1. $^{18}$F-FDG PET/CT could be used as an adjunct to the clinical management of high-risk atherosclerosis and an in vivo tool to study plaque biology.

**Key Words:** atherosclerosis; $^{18}$F-FDG; PET; CT; matrix metalloproteinase-1

**J Nucl Med 2007; 48:227–233**

Cardiovascular events are the leading cause of death in developed countries worldwide. The disruption of atherosclerotic plaques and the subsequent formation of thrombi are currently recognized as the major cause of morbidity and mortality in cardiovascular diseases, including acute ischemic stroke (*1*). The detection of vulnerable plaques is clinically important for risk stratification and treatment. Several imaging approaches have been adapted to detect vulnerable plaques, including conventional x-ray contrast angiography, ultrasonography, high-resolution CT, and MRI. However, most of these techniques are based on morphologic characteristics of atheroma (*2–6*) and do not provide biologic information, such as inflammation.

Inflammation plays a significant role in the pathogenesis, progression, and subsequent plaque rupture in atherosclerosis (*7,8*). Many inflammatory biomarkers have been reported to provide information about the risk of developing cardiovascular disease (*9*). The macrophages are important cellular components of vulnerable plaques. They are also the target of $^{18}$F-FDG and the source of matrix metalloproteinase (MMP) production (*7,10*). Detection of atherosclerotic lesions has been reported using $^{18}$F-FDG taken up by macrophages and vascular smooth muscle cells. This might contribute to the identification of a subgroup of patients at high risk for complications (*11–13*).

However, little is known about the relationship between these circulating inflammatory biomarkers and arterial vascular $^{18}$F-FDG uptake. PET/CT is now emerging as a promising modality in providing better localization and, concurrently, detecting calcification of plaques (*14–18*). In this study, we investigated the clinical relationship between $^{18}$F-FDG PET/CT of carotid atherosclerotic plaques and circulating inflammatory biomarkers in subjects with or without carotid stenosis.

## MATERIALS AND METHODS

### Subjects

We studied 25 consecutive symptomatic subjects with ultrasonographically documented carotid stenosis $\geq$ 70% who were scheduled for elective angiography between March 2004 and July 2005 (*19,20*). Patients with a history of ischemic cerebral stroke, transient ischemic attack (TIA), or amaurosis fugax were classified as symptomatic. Symptoms that developed or progressed within 6 wk were classified as recent onset. The exclusion criteria

Received Aug. 25, 2006; revision accepted Nov. 13, 2006.

For correspondence or reprints contact: Wei-Shiung Yang, MD, PhD, Graduate Institute of Clinical Medicine, College of Medicine, National Taiwan University, No. 1 Chang-Te St., Taipei, 10002, Taiwan.

E-mail: wsyang@ha.mc.ntu.edu.tw

included acute cerebral infarction within 1 mo, cerebral hemorrhage within 6 mo, major surgery or bleeding within 6 mo, and fasting plasma glucose level > 120 mg/dL. At the time of enrollment, the patients were allowed to take aspirin and medications including statin, antidiabetic, or antihypertension drugs with stable doses for at least 1 mo.

Twenty-two apparently healthy subjects referred from the Health Management Center of National Taiwan University Hospital to receive $^{18}$F-FDG PET/CT studies for cancer screening during the same period were used as the control subjects. None had cardiovascular diseases or diabetes mellitus. All control subjects had normal carotid and vertebral arteries documented by ultrasound examination within 1 wk of PET/CT studies. The study was approved by the institutional review board, and written informed consent was obtained from each patient before enrollment.

### Patient Management

Selective cerebral digital subtraction angiography was performed via the femoral artery, starting with imaging of the aortic arch; this was followed by selective injections in the common carotid, subclavian, and vertebral arteries. The severity of extracranial carotid stenosis was measured using the North American Symptomatic Carotid Endarterectomy Trial criteria, as the diameter of the most severe stenosis divided by the diameter of the distal cervical internal carotid artery beyond the stenosis (*21*). The indication for stenting was ≥50% stenosis in diameter for symptomatic lesions and ≥80% in asymptomatic lesions (*19–21*). Any event occurring during admission was recorded as periprocedural. New neurologic deficits or death occurring during the follow-up was documented as a late event. A neck ultrasound study was performed at 1 wk, at 1, 3, and 6 mo, and then annually after the procedure (*19,20*).

### PET/CT Technique

Subjects were asked to fast at least 4 h before $^{18}$F-FDG (333–407 MBq) PET/CT was performed at 45 and 150 min after the $^{18}$F-FDG injection. The whole blood glucose level was measured before $^{18}$F-FDG injection and all subjects had a level ≤ 115 mg/dL.

The scan was performed using an integrated PET/CT device (Discovery LS; GE Healthcare) composed of a dedicated PET scanner with a full-ring bismuth germinate detector and a 16-slice CT scanner. Nonenhanced low-dose CT data were acquired with the following parameters: tube rotation time, 0.5 s per revolution; 140 kV; 80 mA; 22.5 mm per rotation; slice pitch of 6; and slice thickness of 5 mm. PET emission data were acquired in 2-dimensional mode, using a matrix of 128 × 128, followed by reconstruction using ordered-subset expectation maximization. Emission counts were collected over 4 min per table position. Adjacent fields of view shared 1 overlapping slice. A regional scan of the neck was performed immediately after whole-body scanning in 15-cm fields of view with an emission duration of 15 min.

All CT images were reconstructed onto a 512 × 512 matrix, and these data were converted into 511-keV equivalent attenuation factors for attenuation correction. Matched CT and PET image were reconstructed with a field of 500 mm and 4.25-mm slice thickness. An iterative reconstruction and CT-based attenuation correction were used for the PET images.

### Image Analysis

The PET and CT datasets were transferred to a personal computer–based workstation (Xeleris; GE Healthcare) by DICOM (Digital Imaging and Communications in Medicine) transfer. All images were reviewed with dedicated software (eNTEGRA; GE Healthcare) in axial, coronal, and sagittal planes. Two experienced readers reviewed the images without knowledge of the subject's identity.

Vascular calcification was assessed with nonenhanced CT. The greatest protrusion into the lumen was measured on transaxial images and graded as follows: 0, no calcification; 1, thickness < 4 mm; 2, 4–8 mm; and 3, > 8 mm (*14*).

For each subject, early and delayed PET images were evaluated side by side. $^{18}$F-FDG uptake was assessed visually by noncorrected, attenuation-corrected, as well as rotating maximum-intensity projection images. The pattern of $^{18}$F-FDG uptake was recorded as focal, linear, or bandlike on coronal PET images (*14–16*). A standardized uptake value (SUV) normalized for lean body mass was calculated from the 45- and 150-min images. A region of interest (ROI) of 3 × 3 pixels was manually placed on the vascular wall in the transaxial image surrounding the most intense area of $^{18}$F-FDG uptake. The maximum SUV (SUVmax) was recorded using the maximum pixel activity within the ROI. The delayed images provided better lesion-to-background contrast during visual assessment. However, the pattern and locations of $^{18}$F-FDG uptake could be identified in early and in delayed images in all patients with significant carotid stenosis. Because the $^{18}$F-FDG uptake on delayed images greatly decreased in the control subjects, making it difficult for ROI placement along the arterial wall, we used the SUV on 45-min images for comparison. If no definite positive $^{18}$F-FDG uptake was identified within a segment, the SUVmax values were measured along randomly chosen vessel walls.

### Biomarker Measurements

Blood sampling was done with ≥12-h fasting. Peripheral venous blood samples before the diagnostic angiography and immediately after the stenting procedure were collected in patients with carotid artery stenosis. In control subjects, venous blood samples were taken on the day of the ultrasound examinations of the neck. The samples were collected with potassium ethylenediaminetetraacetic acid tubes, and serum was stored at −80°C until assayed. Serum high-sensitivity C-reactive protein (hs-CRP) was measured by a chemiluminescent enzyme-labeled immunometric assay (Immulite C-Reactive Protein; Diagnostic Products Co.). The lowest detectable level of the hs-CRP assay was 0.01 mg/dL. MMP-1 was determined with a commercially available enzyme-linked immunosorbent assay, using the Biotrak Assay System (Amersham).

### Statistical Analysis

Data are expressed as mean ± SD. Comparisons between groups were made using the Student $t$ test and $\chi^2$ analysis or the Mann–Whitney $U$ test for continuous and categoric variables, respectively. The strength of associations was estimated by the Pearson correlation coefficient ($R$). For patients undergoing intervention, biomarkers before and after intervention were compared by a paired $t$ test. A $P$ value < 0.05 was predetermined to be statistically significant. All analyses were conducted using Stata 8 software packages (Stata).

## RESULTS

### Clinical Information

The study population was composed of 25 carotid stenotic subjects and 22 control subjects. The demographic

**TABLE 1**
Baseline Data of Study Subjects

| Parameter | Carotid stenosis ($n$ = 25) | Control subjects ($n$ = 22) | $P$ |
|---|---|---|---|
| Age (y) | 70 ± 8 | 50 ± 10 | <0.001 |
| Male (%) | 23 (92) | 13 (59) | <0.001 |
| Fasting glucose (mg/dL) | 105 ± 17 | 92 ± 13 | NS |
| T-CHO (mg/dL) | 190 ± 42 | 204 ± 40 | NS |
| TG (mg/dL) | 160 ± 95 | 154 ± 170 | NS |
| Leukocyte count (1,000/μL) | 6.3 ± 1.5 | 5.3 ± 1.0 | 0.005 |
| hs-CRP (mg/dL) | 2.2 ± 1.7 | 1.1 ± 1.1 | NS |
| MMP-1 (ng/mL) | 7.6 ± 6.4 | 2.5 ± 1.3 | <0.001 |

NS = nonsignificant between 2 groups; T-CHO = total cholesterol; TG = triglycerides.

characteristics of patients and control subjects are listed in Table 1. The patients with carotid artery stenosis were older and predominantly male. Four patients (16%) had well-controlled diabetes mellitus, 22 (88%) had hypertension, and 7 (28%) were on statin therapy. In contrast, only 4 (18%) of the control group received antihypertensive treatment. The clinical presentations of carotid stenosis among the patient group were amaurosis fugax in 2 (8%) and ischemic stroke or TIA in 18 (72%). Thirteen (52%) patients had symptoms of recent onset or progression within 6 wk. Ten (40%) had concomitant coronary artery disease. The carotid stenosis was bilateral in 5 patients (20%).

Nineteen of 25 patients (76%) underwent stenting in this admission. The procedure was not performed because of minor stenosis of only 50% in 1 asymptomatic lesion, total occlusion in 2, and severe ipsilateral intracranial stenosis in 2 subjects on the angiogram, and a recent head injury in 1 patient. No periprocedural event occurred. Ten patients underwent staged angioplasty for other extracranial arterial stenosis within 6 mo. The average follow-up after the index procedures was 16 ± 3 mo (range, 12–24 mo). No symptomatic or angiographic recurrence occurred during follow-up.

### PET/CT Analyses

Among the 25 subjects with carotid stenosis, the pattern of $^{18}$F-FDG uptake in the aorta was linear in 20 (80%), bandlike in 1, and focal in 4 (3 in aortic arch and 1 in ascending aorta) on coronal views. In the neck regions, $^{18}$F-FDG uptake was linear in 15 (60%), bandlike in 1, and focal in the other 9. None of the control subjects exhibited obvious $^{18}$F-FDG uptake in whole-body scans by visual assessment (Fig. 1).

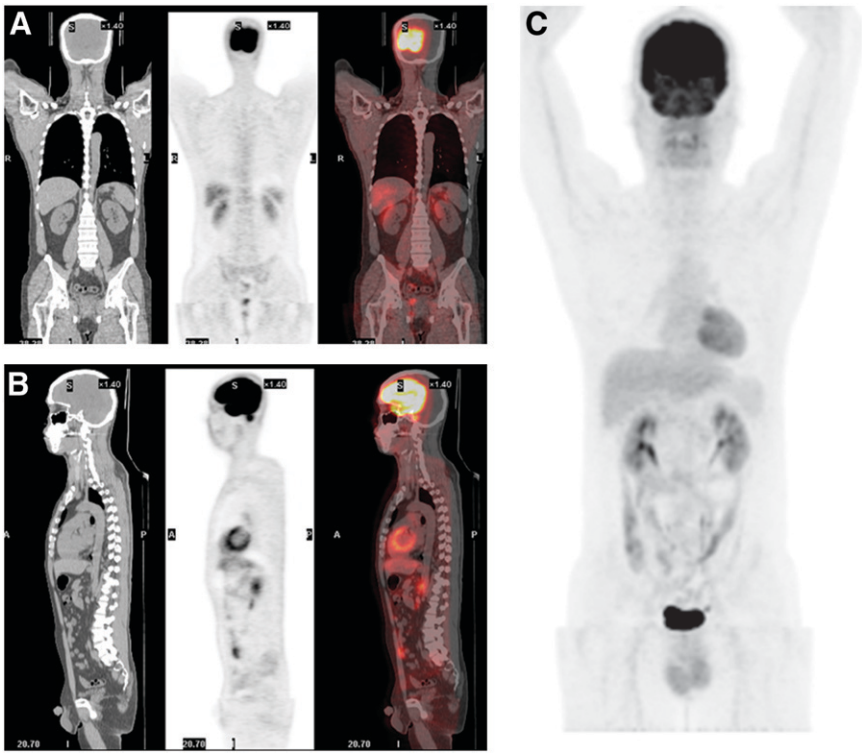


**FIGURE 1.** Coregistered CT (left), $^{18}$F-FDG PET (middle), and fused PET/CT (right) images of coronal (A) and sagittal (B) views and maximal-intensity-projection image (C) from 44-y-old male control subject. No discernable $^{18}$F-FDG uptake is seen in whole vascular system.

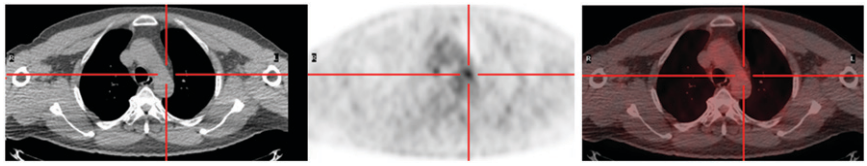

**FIGURE 2.** Transaxial CT (left), $^{18}$F-FDG PET (middle), and fused PET/CT (right) images. Focal $^{18}$F-FDG uptake without significant calcifications is demonstrated in aortic arch from 50-y-old man with significant stenosis of right internal carotid artery, suggesting high level of inflammation activity within this soft plaque.

Higher SUVs along the arterial walls on whole-body scans were observed in the patients with carotid stenosis (mean, 2.1 ± 0.5; range, 1.5–4.4), whereas none of the control subjects had SUVs higher than 2.0 (mean, 1.5 ± 0.3; range, 0.7–2.0) in any major vascular beds ($P < 0.005$). Positive $^{18}$F-FDG uptake or the highest SUV was not consistently located at the sites of calcification. Representative images are shown in Figures 2 and 3.

### Biomarkers

The leukocyte counts and MMP-1 were significantly higher in subjects with carotid stenosis than in the control subjects (Table 1). The values of hs-CRP tended to be higher in patients with carotid stenosis but were not statistically different ($P = 0.06$). This could be caused by the small sample size. In addition, hs-CRP correlated well with leukocyte counts ($r = 0.45$, $P = 0.005$) in all subjects but not with MMP-1 levels.

We also checked the MMP-1 and hs-CRP immediately after intervention (within 30 min) among the 19 subjects who underwent carotid stenting. The MMP-1 level increased immediately after intervention (from 6.2 ± 6.7 to 12.3 ± 8.9 ng/mL, $P = 0.0001$) but not hs-CRP (from 2.2 ± 1.6 to 2.3 ± 1.5 ng/mL, $P =$ not significant). This finding suggests that the rapid surge in the MMP-1 level could be due to plaque disruption by stenting.

Because none of the control subjects had SUV values > 2.0 on the 45-min image over major arteries, the threshold SUVmax of 2 was used for the subsequent analyses. Among the patients with carotid stenosis, the MMP-1 values were significantly higher in patients with a higher SUVmax (>2.0) on the target lesions. Of the 19 patients who underwent successful stenting, postprocedural MMP-1 levels were also significantly higher in those with higher SUVmax values on the target lesions (Fig. 4). The change in MMP-1 levels tended to be greater among the subjects with SUVmax values > 2.0 on target lesions, compared with those with the SUVmax values ≤ 2.0. However, the difference did not reach statistical significance (5.8 ± 3.0 vs. 4.7 ± 0.3 ng/mL, $P = 0.3$), probably due to the small sample size. In contrast, there was no significant correlation between hs-CRP or leukocyte counts among these subjects (data not shown). There also was no difference in these 2 biomarkers between subjects grouped by the SUVmax of target lesions (Table 2).

## DISCUSSION

In the present study, we investigated the relationship between the accumulation of $^{18}$F-FDG on the carotid plaques and circulating levels of inflammatory biomarkers. In patients with established carotid stenosis, vascular $^{18}$F-FDG uptake and calcification were rather common, whereas the distributions of $^{18}$F-FDG uptake and calcification sites were not always compatible. Higher circulating MMP-1 in carotid stenosis patients and its surge after stenting suggested that MMP-1 is an important component of plaques. In addition, patients with higher $^{18}$F-FDG uptake in the carotid lesions also had higher baseline and postintervention serum MMP-1 levels, implying that the composition of plaques could be assessed noninvasively by $^{18}$F-FDG PET/CT.

Inflammation is important in the pathogenesis and progression of atherosclerosis. Plaques containing numerous macrophages are at a higher risk for rupture (*7,8*). $^{18}$F-FDG is a glucose analog that is taken up by cells in proportion to

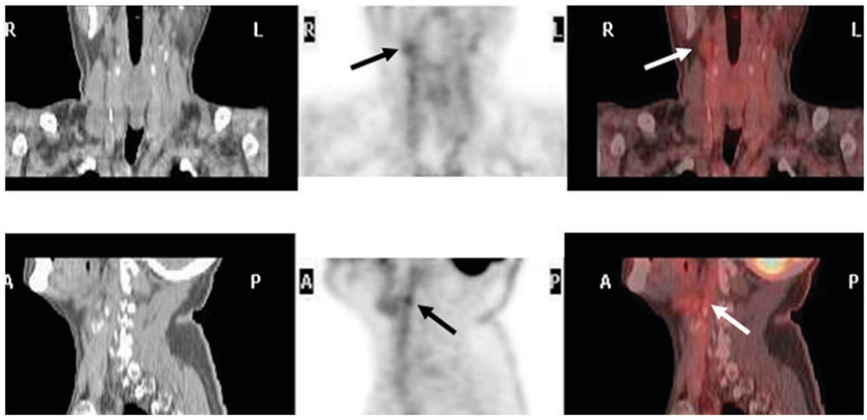


**FIGURE 3.** CT (left), $^{18}$F-FDG PET (middle), and fused PET/CT (right) images of coronal (upper panel) and sagittal (lower panel) view from 75-y-old man, diagnosed with a right carotid territory stroke 1 mo earlier, with a nearly total occlusion of right common and internal carotid artery and 70% luminal stenosis of left common carotid artery on angiogram. Calcifications are seen in the neck bilaterally, whereas the most intense $^{18}$F-FDG uptake was demonstrated over the right carotid artery region (arrows). Highly inflammatory right carotid artery plaque could be the cause of this patient's presenting symptoms.

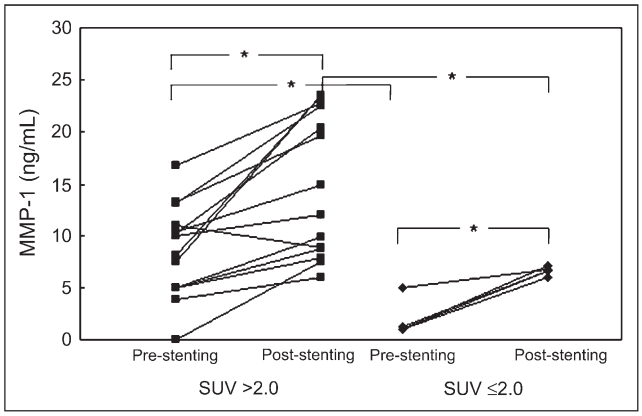


**FIGURE 4.** Baseline and postprocedural MMP-1 levels in patients with target lesion SUVmax $>$ 2 (left) and $\leq$ 2 (right). *$P < 0.05$.

their metabolic activity. Several articles have reported the potential roles of metabolic imaging in the assessment of inflammatory vascular diseases (*11–13,16–18,22*). $^{18}$F-FDG uptake in atherosclerotic aortic aneurysms (*23*) and carotid stenosis (*13*) appears to correlate with a worse prognosis. Furthermore, changes in $^{18}$F-FDG activity in response to treatment occurred earlier than morphologic changes (*24*). Animal models also demonstrated that the accumulation of $^{18}$F-FDG is located at the regions of extensive inflammatory cellular infiltration (*25–28*). These data support the idea that $^{18}$F-FDG PET could be a noninvasive tool to identify the hypermetabolic state of inflammatory atheromas, which contributes to the vulnerability of atherosclerotic plaques (*28–30*).

In our study, we found higher $^{18}$F-FDG uptake, and calcifications were common in patients with documented carotid stenosis (*16–18*), suggesting concurrent extensive and advanced atherosclerosis (*31*). The different distributions of $^{18}$F-FDG uptake and calcifications may reflect the different stages of atherosclerosis progression. Even in the locations without obvious calcification or plaque seen in noncontrasted CT, higher $^{18}$F-FDG uptake may suggest a higher potential for atherosclerosis occurrence or progression (*22*).

Ruptured plaques characteristically contain numerous macrophages producing MMPs capable of degrading the extracellular matrix. Overexpression of these enzymes has been reported to lead to thinning of the fibrous cap and to subsequent plaque rupture (*18,32–38*). Imaging of MMP activity by radiolabeled molecules has been reported (*39*); however, it is still far from clinical application. On the other hand, $^{18}$F-FDG is the most popular PET tracer. In the present study, we demonstrated the relationship between $^{18}$F-FDG uptake activity and the circulating MMP-1 levels in patients with carotid stenosis. To our knowledge, this is the first study showing the relationship between circulating MMP-1 levels and $^{18}$F-FDG PET. Although the leukocyte count and hs-CRP level also tended to be higher in patients with carotid stenosis, there was no significant correlation between $^{18}$F-FDG activity and these 2 markers. It appears that MMP-1, a more specific marker of local plaque inflammation, correlates better with focal $^{18}$F-FDG uptake, rather than the systemic inflammatory markers such as leukocyte count and hs-CRP.

In our study, the MMP-1 increased immediately after intervention but not the hs-CRP. Previous studies reported

**TABLE 2**
Comparison of Biomarker Levels Between Subjects with High and Those with Low SUVmax Values of Carotid Lesions in All Subjects with Carotid Stenosis and in Those Who Underwent Stenting

| All patients with carotid stenosis ($n$ = 25) | | | |
|---|---|---|---|
| Baseline | SUVmax $>$ 2.0 ($n$ = 18) | SUVmax $\leq$ 2.0 ($n$ = 7) | $P$ |
| hs-CRP (mg/dL) | 2.0 ± 1.6 | 2.4 ± 1.3 | NS |
| MMP-1 (ng/mL) | 9.3 ± 6.0 | 1.4 ± 3.1 | 0.01 |
| Leukocyte count (1,000/μL) | 6.4 ± 1.5 | 6.3 ± 0.9 | NS |
| **Patients who underwent stenting ($n$ = 19)** | | | |
| Parameter | SUVmax $>$ 2.0 ($n$ = 14) | SUVmax $\leq$ 2.0 ($n$ = 5) | $P$ |
| hs-CRP (mg/dL) | | | |
| Baseline | 2.1 ± 1.6 | 2.6 ± 1.4 | NS |
| After stenting | 2.1 ± 1.7 | 2.7 ± 1.5 | NS |
| MMP-1 (ng/mL) | | | |
| Baseline | 7.6 ± 6.7 | 1.9 ± 1.2 | 0.02 |
| After stenting | 14.1 ± 8.8 | 6.6 ± 0.5 | 0.03 |
| Leukocyte count (1,000/μL) | | | |
| Baseline | 6.5 ± 1.9 | 5.8 ± 0.7 | NS |
| Second day | 8.4 ± 1.9 | 7.2 ± 1.6 | NS |

NS = nonsignificant between 2 groups.

that serum inflammatory factors, such as hs-CRP, increased after intervention. In these studies, the timing of measurements was 6 h or more after the interventions (*40–42*). The sampling time difference could explain the discrepancies of changes in hs-CRP, MMP-1, and leukocyte count between our study and other studies. In our study, the rapid surge of MMP-1 after the intervention was most likely caused by disruption of plaques by stenting, not by a systemic inflammatory response.

Determination of $^{18}$F-FDG uptake for discriminating stable and vulnerable plaques is of clinical importance. It could be applied to assessing the risk of plaque rupture and also to monitoring the therapeutic effects. Although atherosclerotic plaques could be small, our results demonstrate that the integrated use of PET/CT is helpful in overcoming the problems of PET lacking anatomic information and its lower spatial resolution. Our results also showed that vascular $^{18}$F-FDG activity was low in the control subjects. The correlation between MMP-1 levels and $^{18}$F-FDG accumulation suggests the potential of $^{18}$F-FDG PET in selective cases for assessing the vulnerability of plaques. The patients with target lesions of SUVmax $>$ 2.0 tended to have a higher baseline and poststenting surge of MMP-1, although the periprocedural surge did not reach statistical significance, probably because of the small sample size. Nevertheless, the role of $^{18}$F-FDG PET in prediction of periprocedural complications during stenting also warrants further evaluation.

There were some limitations to this study. Age and sex are not well matched between the patients and the control subjects. The sample size was relatively small. Patients having a cerebral infarction within 1 mo were excluded in the present study. This may partially explain why the intensity of $^{18}$F-FDG uptake tended to be lower than that in previous reports (*12,13*). We did not have any information with regard to the histopathology of the plaques in this study. The clinical significance of the $^{18}$F-FDG uptake and the changes in inflammatory markers are not yet clear from this study. However, further prospective large-scale evaluation is warranted. The spatial resolution of PET/CT is still limited in relating the size and specific sites of plaques. In addition, low-dose nonenhanced CT also limited the resolution of the soft tissue, including soft plaques.

## CONCLUSION

Our study showed that $^{18}$F-FDG PET/CT can depict metabolically active atherosclerotic plaques, and patients with higher $^{18}$F-FDG uptake also had higher circulating MMP-1. Thus, $^{18}$F-FDG PET/CT could be used as a noninvasive imaging modality in detecting and monitoring the atherosclerotic process.

## ACKNOWLEDGMENTS

We acknowledge help from the Health Management Center of National Taiwan University Hospital. We also thank Chien-Chung Chen, Yu-Chiao Chi, and Yu-Ping Ho for technical assistance. The work was supported in part by grant NTUH 94-N04 from the National Taiwan University Hospital and by grant NSC-94-2314-B-002-185 from the National Science Council of Taiwan.

## REFERENCES

1. Murray CJ, Lopez AD. Alternative projections of mortality and disability by cause 1990–2020: Global Burden of Disease study. *Lancet.* 1997;349:1498–1504.
2. Celermajer DS. Noninvasive detection of atherosclerosis. *N Engl J Med.* 1998; 39:2014–2015.
3. Fayad ZA, Fuster V. Clinical imaging of the high-risk or vulnerable atherosclerotic plaque. *Circ Res.* 2001;89:305–316.
4. Fayad ZA, Fuster V, Nikolaou K, Becker C. Computed tomography and magnetic resonance imaging for noninvasive coronary angiography and plaque imaging: current and potential future concepts. *Circulation.* 2002;106:2026–2034.
5. Rudd JH, Davies JR, Weissberg PL. Imaging of atherosclerosis: Can we predict plaque rupture? *Trends Cardiovasc Med.* 2005;15:17–24.
6. Jaffer FA, Libby P. Weissleder R. Molecular and cellular imaging of atherosclerosis: emerging applications. *J Am Coll Cardiol.* 2006;47:1328–1338.
7. Libby P. Inflammation in atherosclerosis. *Nature.* 2002;420:868–874.
8. Lombardo A, Biasucci LM, Lanza GA, et al. Inflammation as possible link between coronary and carotid plaque instability. *Circulation.* 2004;109:3158–3163.
9. Pearson TA, Mensah GA, Alexander RW, et al. Markers of inflammation and cardiovascular disease: application to clinical and public health practice—A statement for healthcare professionals from the Centers for Disease Control and Prevention and the American Heart Association. *Circulation.* 2003;107: 499–511.
10. Galis ZS, Khatri JJ. Matrix metalloproteinases in vascular remodeling and atherogenesis: the good, the bad, and the ugly. *Circ Res.* 2002;90:251–262.
11. Yun M, Jang S, Cucchiara A, Newberg AB, Alavi A. $^{18}$F-FDG uptake in the large arteries: a correlation study with the atherogenic risk factors. *Semin Nucl Med.* 2002;32:70–76.
12. Rudd JH, Warburton EA, Fryer TD, et al. Imaging atherosclerotic plaque inflammation with [$^{18}$F]-fluorodeoxyglucose positron emission tomography. *Circulation.* 2002;105:2708–2711.
13. Davies JR, Rudd JH, Fryer TD, et al. Identification of culprit lesions after transient ischemic attack by combined $^{18}$F fluorodeoxyglucose positron emission tomography and high-resolution magnetic resonance imaging. *Stroke.* 2005;36: 2642–2647.
14. Schwaiger M, Ziegler S, Nekolla SG. PET/CT: challenge for nuclear cardiology. *J Nucl Med.* 2005;46:1664–1678.
15. von Schulthess GK, Steinert HC, Hany TF. Integrated PET/CT: current applications and future directions. *Radiology.* 2006;238:405–422.
16. Tatsumi M, Cohade C, Nakamoto Y, Wahl RL. Fluorodeoxyglucose uptake in the aortic wall at PET/CT: possible finding for active atherosclerosis. *Radiology.* 2003;229:831–837.
17. Ben-Haim S, Kupzov E, Tamir A, Israel O. Evaluation of $^{18}$F-FDG uptake and arterial wall calcifications using $^{18}$F-FDG PET/CT. *J Nucl Med.* 2004;45:1816–1821.
18. Dunphy MP, Freiman A, Larson S, Strauss HW. Association of vascular $^{18}$F-FDG uptake with vascular calcification. *J Nucl Med.* 2005;46:1278–1284.
19. Kao HL, Lin LY, Lu CJ, Jeng JS, Yip PK, Lee YT. Long-term results of elective stenting for severe carotid artery stenosis in Taiwan. *Cardiology.* 2002;97:89–93.
20. Lu CJ, Kao HL, Sun Y, et al. The hemodynamic effects of internal carotid artery stenting: a study with color-coded duplex sonography. *Cerebrovasc Dis.* 2003; 15:264–269.
21. The North American Symptomatic Carotid Endarterectomy Trial (NASCET) Steering Committee. North American Symptomatic Carotid Endarterectomy Trial: methods, patient characteristics, and progress. *Stroke.* 1991;22:711–720.
22. Okane K, Ibaraki M, Toyoshima H, et al. $^{18}$F-FDG accumulation in atherosclerosis: use of CT and MR co-registration of thoracic and carotid arteries. *Eur J Nucl Med Mol Imaging.* 2006;33:589–594.
23. Sakalihasan N, Van Damme H, Gomez P, et al. Positron emission tomography (PET) evaluation of abdominal aortic aneurysm (AAA). *Eur J Vasc Endovasc Surg.* 2002;23:431–436.
24. Meller J, Strutz F, Siefker U, et al. Early diagnosis and follow-up or aortitis with [$^{18}$F]FDG PET and MRI. *Eur J Nucl Med Mol Imaging.* 2003;30:730–736.
25. Ogawa M, Ishino S, Mukai T, et al. $^{18}$F-FDG accumulation in atherosclerotic plaques: immunohistochemical and PET imaging study. *J Nucl Med.* 2004;45: 1245–1250.

26. Tawakol A, Migrino RQ, Hoffmann U, et al. Noninvasive in vivo measurement of vascular inflammation with F-18 fluorodeoxyglucose positron emission tomography. *J Nucl Cardiol.* 2005;12:294–301.
27. Zhang Z, Machac J, Helft G, et al. Non-invasive imaging of atherosclerotic plaque macrophage in a rabbit model with F-18 FDG PET: a histopathological correlation. *BMC Nucl Med.* 2006;25(6):3.
28. Laitinen I, Marjamaki P, Haaparanta M, et al. Non-specific binding of [$^{18}$F]FDG to calcifications in atherosclerotic plaques: experimental study of mouse and human arteries. *Eur J Nucl Med Mol Imaging.* 2006;33:1461–1467.
29. Jaffer FA, Weissleder R. Molecular imaging in the clinical arena. *JAMA.* 2005;293:855–862.
30. Davies JR, Rudd JH, Weissberg PL, Narula J. Radionuclide imaging for the detection of inflammation in vulnerable plaques. *J Am Coll Cardiol.* 2006;47: C57–C68.
31. Wu YW, Lin MS, Lin YH, Chao CL, Kao HL. Prevalence of concomitant atherosclerotic arterial diseases in patients with significant cervical carotid artery stenosis in Taiwan. *Int J Cardiovasc Imaging.* November 22, 2006. Available at: http://www.springerlink.com/content/fn725272h6415355/fulltext.html.
32. Galis ZS, Sukhova GK, Lark MW, Libby P. Increased expression of matrix metalloporoteinases and matix degrading activity in vulnerable regions of human atherosclerotic plaques. *J Clin Invest.* 1994;75:181–189.
33. Nikkari ST, O'Brien KD, Ferguson M, et al. Interstitial collagenase (MMP-1) expression in human carotid atherosclerosis. *Circulation.* 1995;92:1393–1398.
34. Sukhova GK, Schönbeck U, Rabkin E, et al. Evidence for increased collagenolysis by interstitial collagenases-1 and -3 in vulnerable human atheromatous plaques. *Circulation.* 1999;99:2503–2509.
35. Ghilardi G, Biondi ML, DeMonti M, Turri O, Guagnellini E, Scorza R. Matrix metalloproteinase-1 and matrix metalloproteinase-3 gene promoter polymorphisms are associated with carotid artery stenosis. *Stroke.* 2002;33:2408–2412.
36. Inoue T, Kato T, Takayanagi K, et al. Circulating matrix metalloproteinase-1 and -3 in patients with an acute coronary syndrome. *Am J Cardiol.* 2003;92: 1461–1462.
37. Morgan AR, Rerkasem K, Gallagher PJ, et al. Differences in matrix metalloproteinase-1 and matrix metalloproteinase-12 transcript levels among carotid atherosclerotic plaques with different histopathological characteristics. *Stroke.* 2004;35:1310–1315.
38. Montero I, Orbe J, Varo N, et al. C-reactive protein induces matrix metalloproteinase-1 and -10 in human endothelial cells: implications for clinical and subclinical atherosclerosis. *J Am Coll Cardiol.* 2006;47:1369–1378.
39. Schafers M, Riemann B, Kopka K, et al. Scintigraphic imaging of matrix metalloproteinase activity in the arterial wall in vivo. *Circulation.* 2004;109: 2554–2559.
40. Franke A, Lante W, Fackeldey V, et al. Pro-inflammatory cytokines after different kinds of cardio-thoracic surgical procedures: Is what we see what we know? *Eur J Cardiothorac Surg.* 2005;28:569–575.
41. Taurino M, Visco V, Raffa S, et al. Matrix metalloproteinase 9 activity in patients before and after endovascular or surgical repair of abdominal aortic aneurysms. *Vascular.* 2004;12:312–317.
42. Ge J, Shen C, Liang C, Chen L, Qian J, Chen H. Elevated matrix metalloproteinase expression after stent implantation is associated with restenosis. *Int J Cardiol.* 2006;112:85–90.